Supporting Information

UV/nitrilotriacetic acid process as a novel strategy for efficient photoreductive degradation of perfluorooctane sulfonate

Zhuyu Sun,[†‡] Chaojie Zhang,*[†‡] Lu Xing,[†‡] Qi Zhou,[†‡] Wenbo Dong,[&] Michael R. Hoffmann[§]

[†]State Key Laboratory of Pollution Control and Resources Reuse, College of Environmental Science and Engineering, Tongji University, Shanghai 200092, China

[‡]Shanghai Institute of Pollution Control and Ecological Security, Shanghai 200092, China

[&]Shanghai Key Laboratory of Atmospheric Particle Pollution and Prevention, Department of Environmental Science & Engineering, Fudan University, Shanghai 200433, China

[§]Linde-Robinson Laboratories, California Institute of Technology, Pasadena, California 91125, United States

*Corresponding author. Tel: +86 21 65981831; fax: +86 21 65983869;

E-mail address: myrazh@tongji.edu.cn.

Number of pages: 20

Number of Figures: 13

Number of Tables: 2

2. Materials and methods

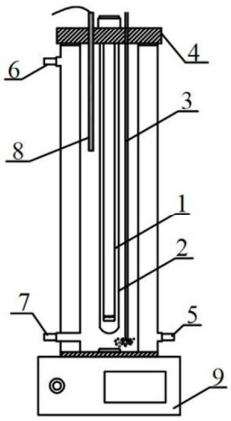

Figure S1. Schematic diagram of the photochemical reactor.

Description of the experimental setup: 1. UV light; 2. Quartz tube; 3. Aeration tube (connected with N_2); 4. Seal snap and silicone seal gasket; 5. Condensate inlet; 6. Condensate outlet; 7. Solution sampling port; 8. Temperature sensor; 9. Electromagnetic stirrer with heating system.

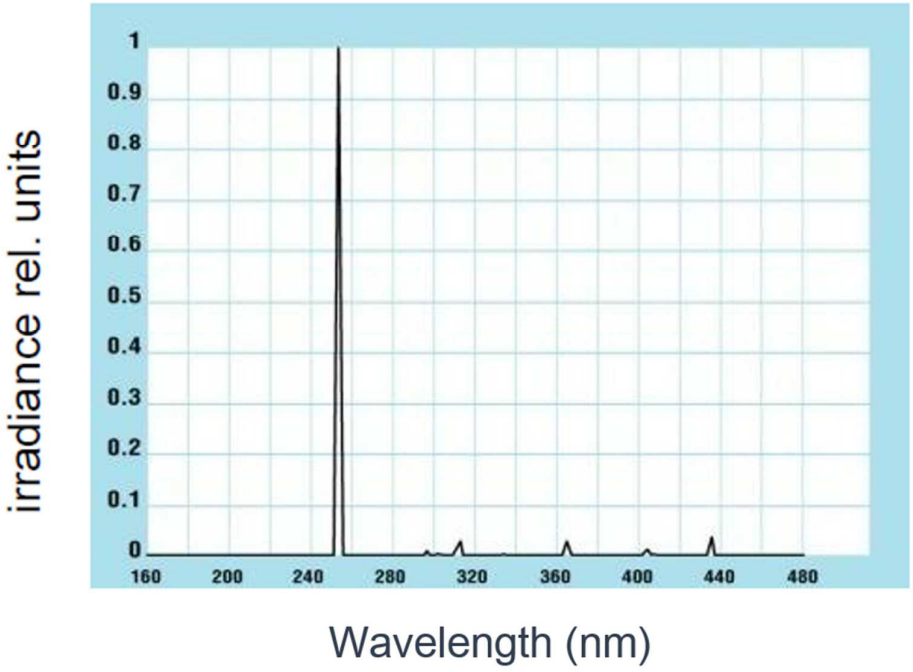

Figure S2. Wavelength distribution of emission from the low-pressure mercury lamp. The technical data are supplied by Heraeus Noblelight (Shenyang) Ltd.

2.3. Analytical methods

(1) LC/MS/MS

Concentrations of PFOS and possible aqueous-phase intermediate analytes were determined by high-performance liquid chromatography/tandem mass spectrometry (HPLC-MS/MS, TSQ^{TM} Quantum Access^{TM}, Thermo Finnigan, San Jose, CA, USA). Aliquots of 10 μL samples were injected onto a 150 mm × 2.1 mm Hyperdil Gold C18 column (3 μm pore size, Thermo Hypersil-Keystone, Bellefonte, PA) by the Surveyor autosampler, and a gradient mobile phase of methanol and 2mM ammonium acetate aquatic solution was delivered at a flow rate of 250 μL min^{-1} by the Surveyor LC Pump. Initial eluent conditions were 10% methanol and kept for 2 min, and the percent methanol increased linearly to 40% at 3 min, ramped to 95% at 9 min, held at 95% for 3 mins, and then reverted to 10% at 15.5 min. The column and tray temperature were maintained at 30 ^{o}C and 4 ^{o}C, respectively. The HPLC tubing made up of polytetrafluoroethylene (PTFE) were replaced with polyetheretherketone (PEEK) tubing and the degasser with fluoropolymer coatings was isolated from HPLC. In order to stabilize the retention times of analytes, helium gas was used for degasification of the mobile phase solvents.

For quantitative determination, the HPLC was interfaced to a Finnigan TSQ™ Quantum Access™ (Thermo Electron, San Jose, CA, USA) triple quadrupole mass spectrometer equipped with electrospray ionization (ESI) source. Electrospray negative ionization was used in the tandem mass spectrometer (MS/MS) ion source. The spray voltage, for all analytes, was set at negative 3200 V. Sheath gas pressure,

ion sweep gas pressure and auxiliary gas pressure were 35 arbitrary units (au), 0 au and 5 au, respectively. Capillary temperature was 320 ^{o}C. Transitions for all ions were observed using selected reaction monitoring (SRM) mode, and analyte-specific mass spectrometer parameters such as parent ions, product ions and collision energies were optimized for each compound.

(2) Ion chromatography

The amount of fluoride, nitrate and short chain organic acid were analyzed by Ion Chromatography (Dionex, IC-3000, Thermo Fisher Scientific, USA) equipped with a conductivity detector and a self-regenerating suppressor. Potassium hydroxide eluent with the flow rate of 1.5 mL/min was achieved. Samples (1.5 mL) were transferred from the reactor to disposable sample vials and sealed with filter caps and loaded onto Automated Sampler. Aliquots of 400 μL samples were injected and separated on a Dionex Ionpac AS11 column (250 mm × 2 mm inner diameter), and then quantified by conductivity detector.

(3) Chromatograms of NTA and its degradation products.

The chromatograms of NTA and its degradation products including IDA, oxamate, oxalate and nitrate are shown in **Fig. S3.**

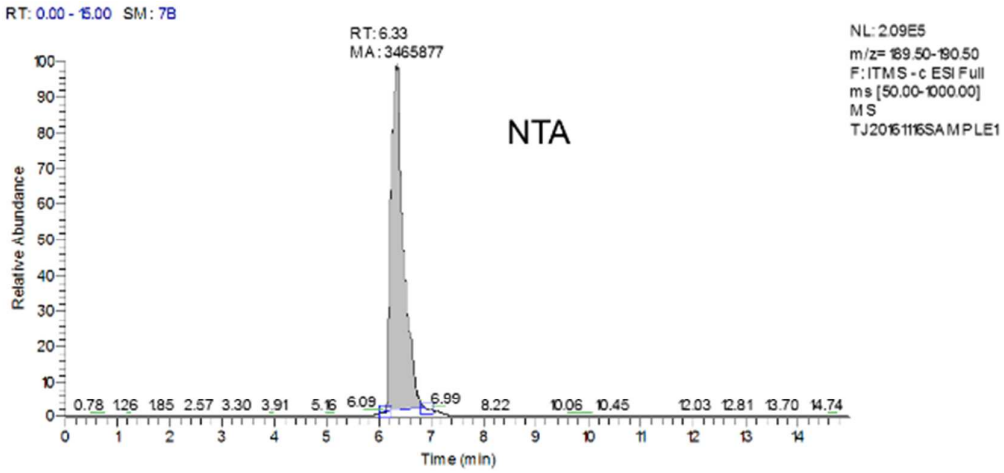
RT: 0.00 - 15.00 SM: 7B
RT: 6.33
MA: 3465877
NTA
NL: 2.09E5
m/z= 189.50-190.50
F: ITMS - c ESI Full
ms [50.00-1000.00]
MS
TJ20161116SAMPLE1
Relative Abundance
Time (min)

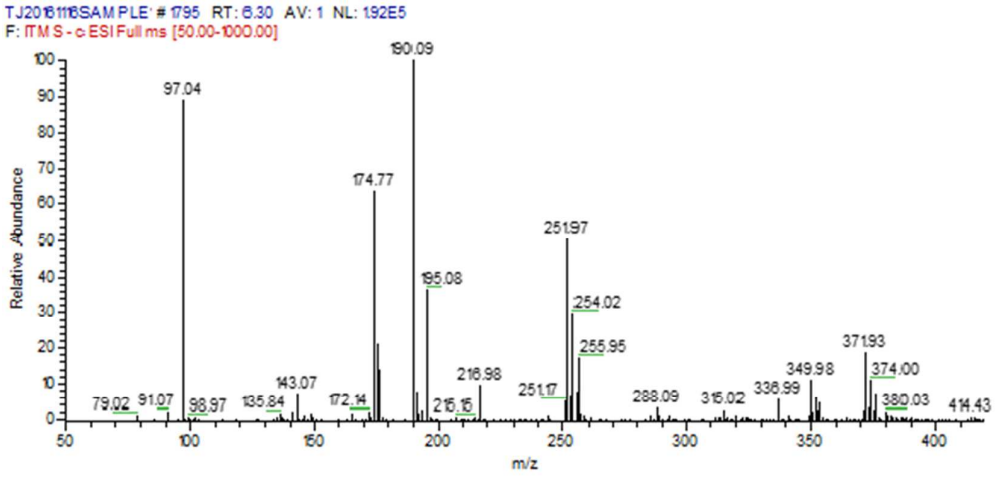
TJ20161116SAMPLE1 # 1795 RT: 6.30 AV: 1 NL: 1.92E5
F: ITMS - c ESI Full ms [50.00-1000.00]
190.09
97.04
174.77
251.97
195.08
254.02
255.95
371.93
349.98
374.00
216.98
143.07
Relative Abundance
m/z

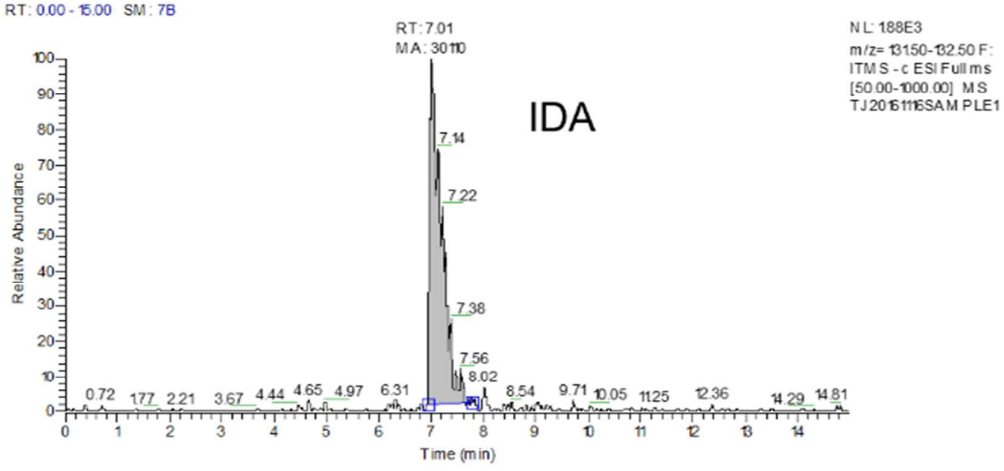
RT: 0.00 - 15.00 SM: 7B
RT: 7.01
MA: 30110
IDA
NL: 188E3
m/z= 131.50-132.50 F:
ITMS - c ESI Full ms
[50.00-1000.00] MS
TJ20161116SAMPLE1
7.14
7.22
7.38
7.56
8.02
Relative Abundance
Time (min)

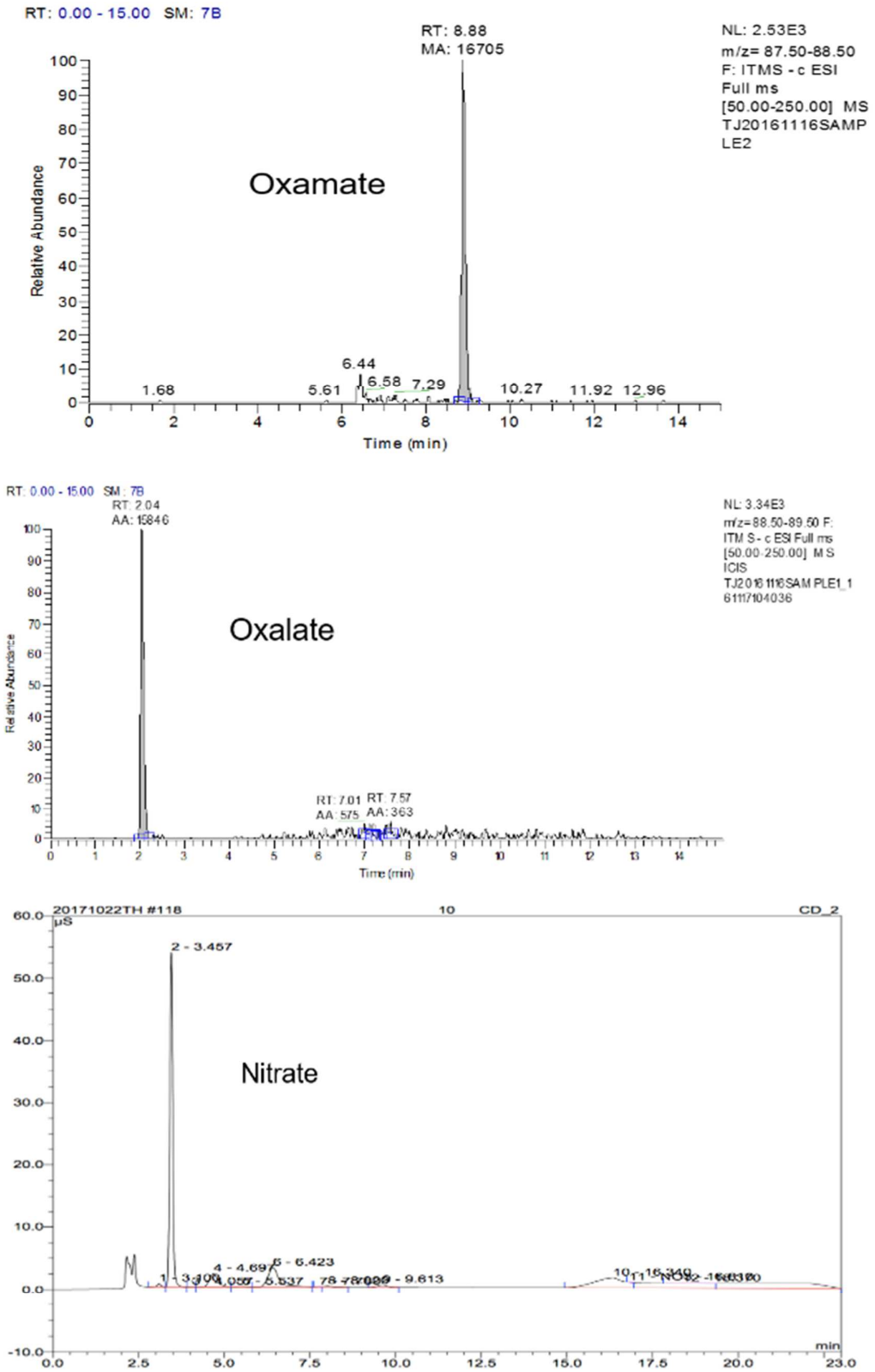

Figure S3. The chromatograms of NTA and its degradation products. NTA, IDA, oxamate and oxalate were detected by LC/MS/MS. Nitrate was detected by ion chromatography.

2.4. Laser flash photolysis experiment and electron spin resonance (ESR) measurement

The laser pulse energy was measured using a Nova PE25BB-SH-V2 pyroelectric head (Ophir Optronics Ltd.). Transient spectra were recorded by the LSK.60 spectrometer (Applied Photophysics Ltd.). The sample solution was placed in a 1 cm × 1 cm quartz cuvette and deaerated by vigorously bubbling with high-purity N_2 (99.99%) for 20 mins. All experiments were performed at 25 ± 1 ^{o}C.

The photochemical experiment for ESR measurement was conducted in a quartz cell. 1.1 mL solution containing 5 mM NTA and 400 mM DMPO (radical trap agent) was added into the vessel after the solution pH was adjusted to 10.0 with $NH_3 \cdot H_2O$-NH_4Cl buffer. Before the reaction, the mixture was bubbled with highly purified nitrogen for 5 mins to remove oxygen. The quartz cell was sealed instantly after its upper part was filled with nitrogen. The reaction was carried out under anoxic conditions to avoid the interference of O_2. The photoreaction was initiated by the 254 nm UV light of a low-pressure mercury lamp (14 W, Heraeus, Germany). After irradiation, 20 μL sample was immediately added into a capillary tube with the internal diameter of 1.0 mm for ESR measurements.

3. Results and Discussion

3.1. NTA-assisted photoreductive degradation and defluorination of PFOS

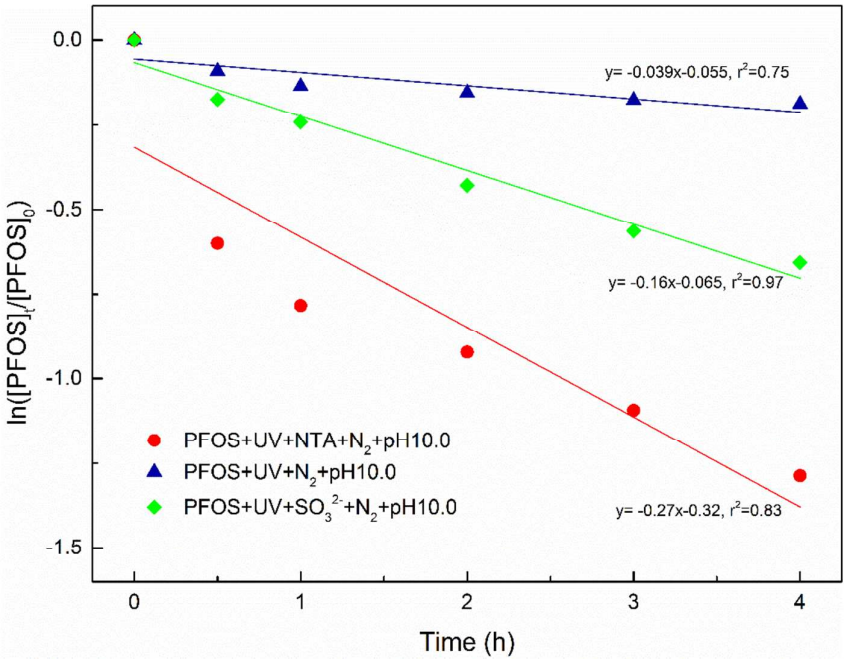

Figure S4. PFOS degradation kinetics under different conditions. Reaction conditions were the same as **Figure 1**.

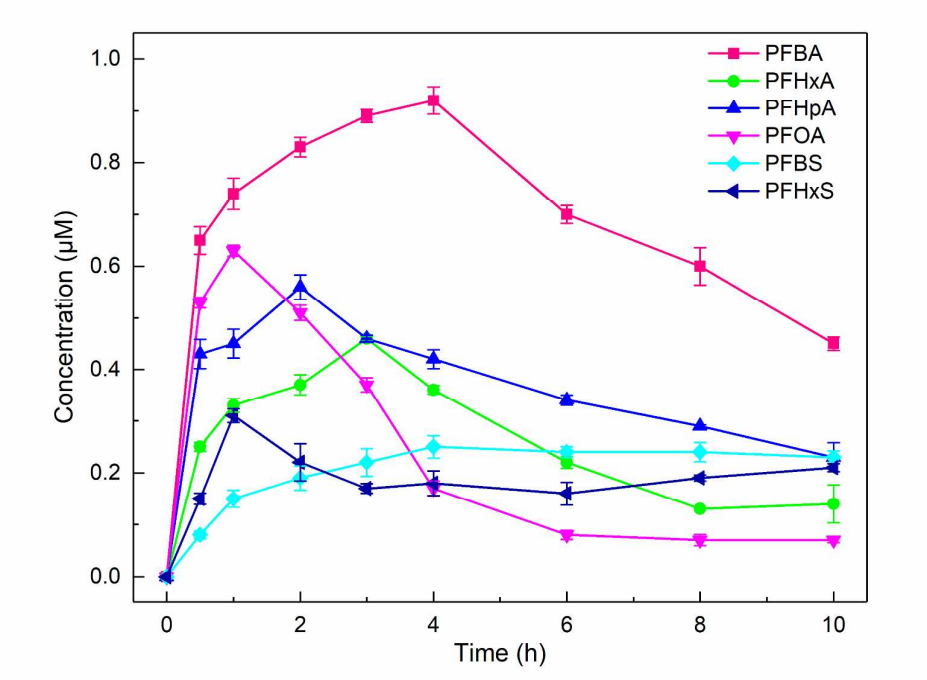

Figure S5. The time profiles of short-chain-length PFAAs intermediates during the photoreductive degradation of PFOS by UV/NTA process.

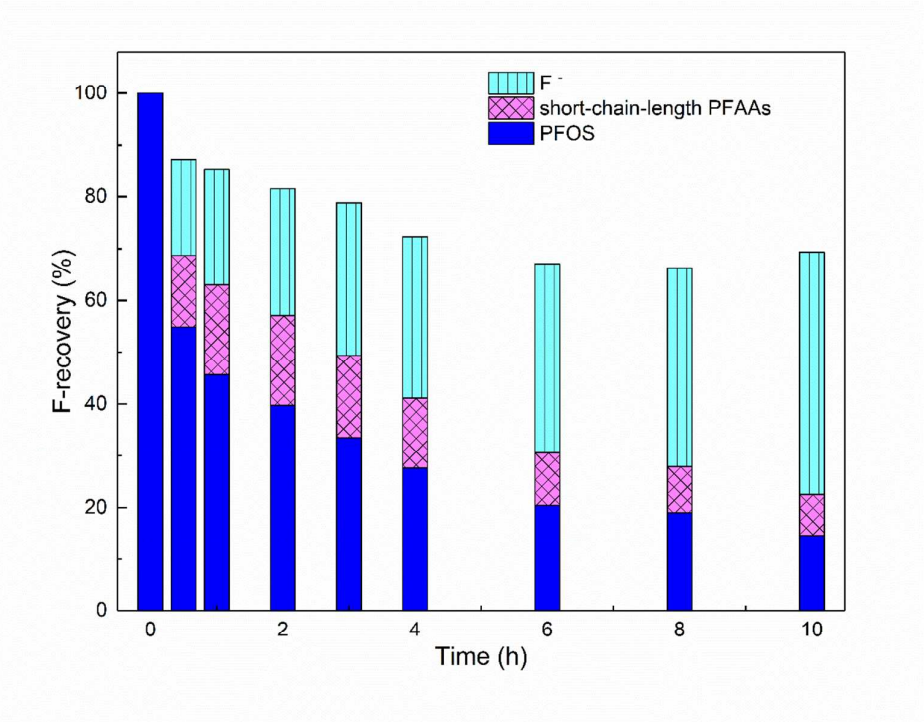

Figure S6. The time dependence of the mass balance of F during the photoreductive degradation of PFOS by UV/NTA process. Formed short-chain-length PFAAs include PFBS, PFBA, PFHxS, PFHxA, PFHpA and PFOA.

Table S1. Comparison of this study with reported photochemical approaches for PFOS degradation in literatures.

Method	Conditions	k^a (h^{-1})	$t_{1/2}{}^b$ (h)	Ref.
UV/NTA	PFOS = 0.01 mM; NTA = 2 mM; λ=254 nm; 14 W low-pressure mercury lamp [c]; pH = 10	0.27	2.6	this study
UV/buffer	PFOS = 0.01 mM; λ=254 nm; 14 W low-pressure mercury lamp; pH = 10	0.039	17.8	this study
UV/sulfite	PFOS = 0.01 mM; SO_3^{2-}= 2 mM; λ=254 nm; 14 W low-pressure mercury lamp; pH = 10	0.16	4.3	this study
UV/alkaline 2-propanol	PFOS = 0.04 mM; λ = 254 nm; 32 W low-pressure mercury lamp	0.039	17.9	1
UV/KI	PFOS = 0.02 mM; KI =10 mM; λ=254 nm; 8 W low-pressure mercury lamp; pH = 6.5	0.18	3.9	2
UV/$K_2S_2O_8$	PFOS = 0.186 mM; $K_2S_2O_8$=18.5 mM; λ = 254 nm; Two 15 W low-pressure mercury lamp; pH = 3.13	0.018	38.5	3
UV/Fe(□)	PFOS = 0.02 mM; Fe(□) = 0.1 mM; λ = 254 nm; 23 W low-pressure mercury lamp;	0.070	9.9	4

a. pseudo-first-order kinetics;

b. half-life time;

c. all methods used low-pressure mercury lamps as the irradiation source to emit UV light at 254 nm.

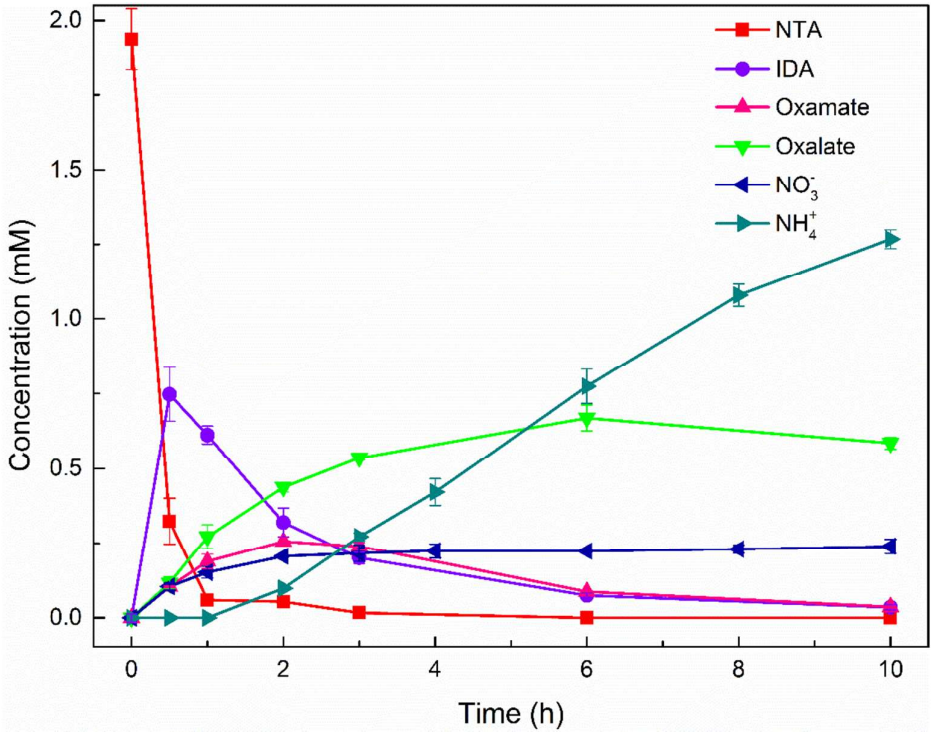

Figure S7. Time profiles of NTA degradation and its degradation products during the photoreductive decomposition of PFOS. PFOS (0.01 mM), NTA (2 mM), UV irradiation (254 nm), N_2 saturated, pH (10.0). Error bars represent standard deviations of triplicate assays.

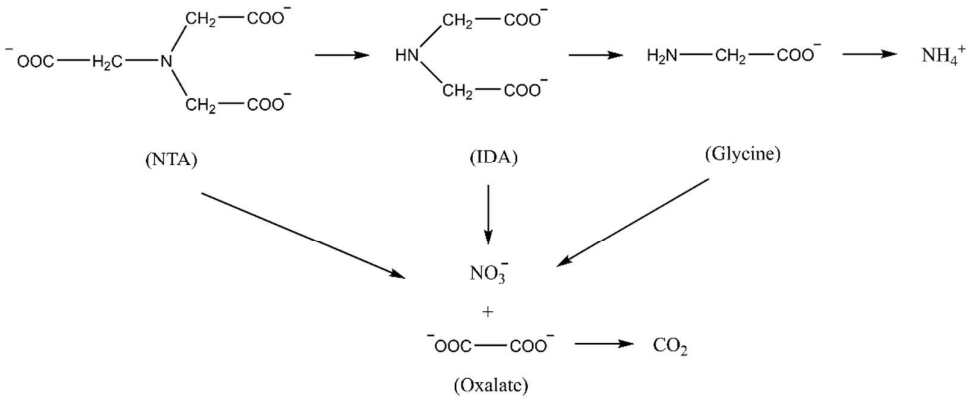

Figure S8. Proposed decomposition pathway of NTA under UV irradiation in this study.

3.2. Mechanism of the NTA-assisted UV photoreductive degradation of PFOS

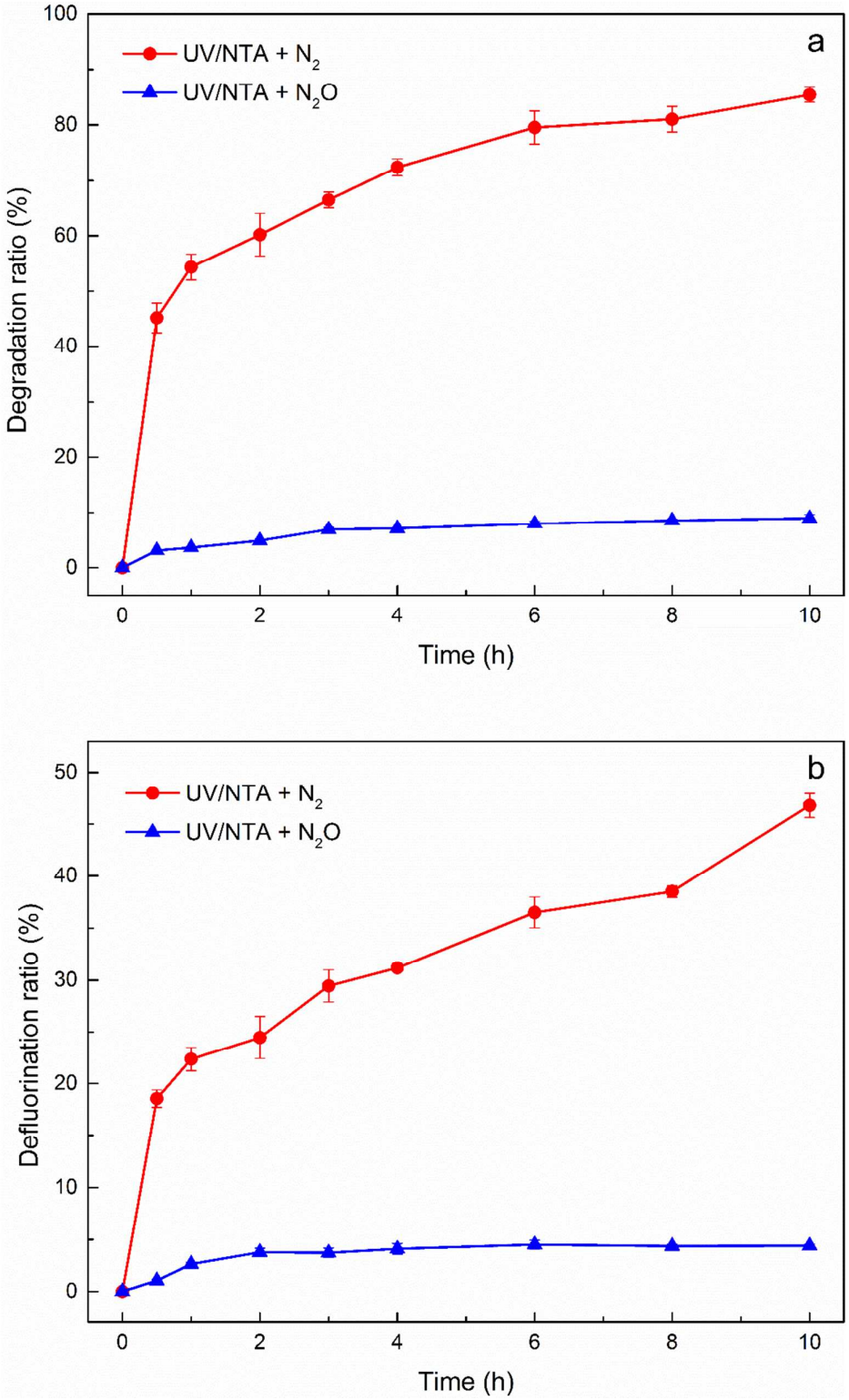

Figure S9. The effect of N_2O on the degradation (**a**) and defluorination (**b**) of PFOS: PFOS (0.01

mM), NTA (2 mM), UV irradiation, pH (10.0). Error bars represent standard deviations of triplicate assays.

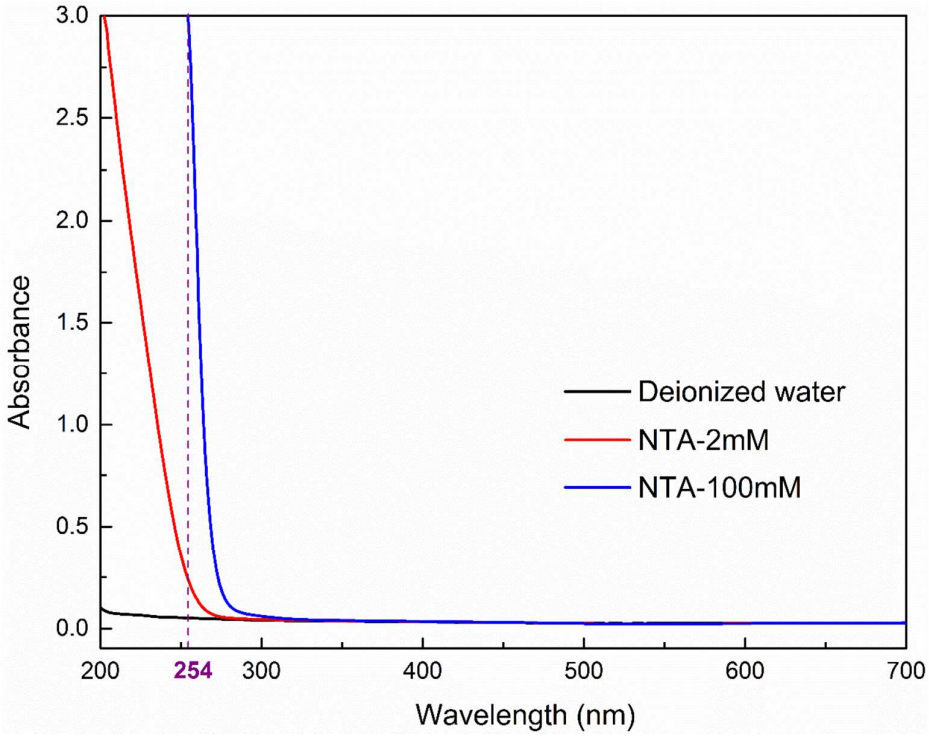

Figure S10. UV-Vis absorption spectra for 2 mM NTA solution (pH = 10.0), 100 mM NTA solution (pH = 12.2) and deionized water.

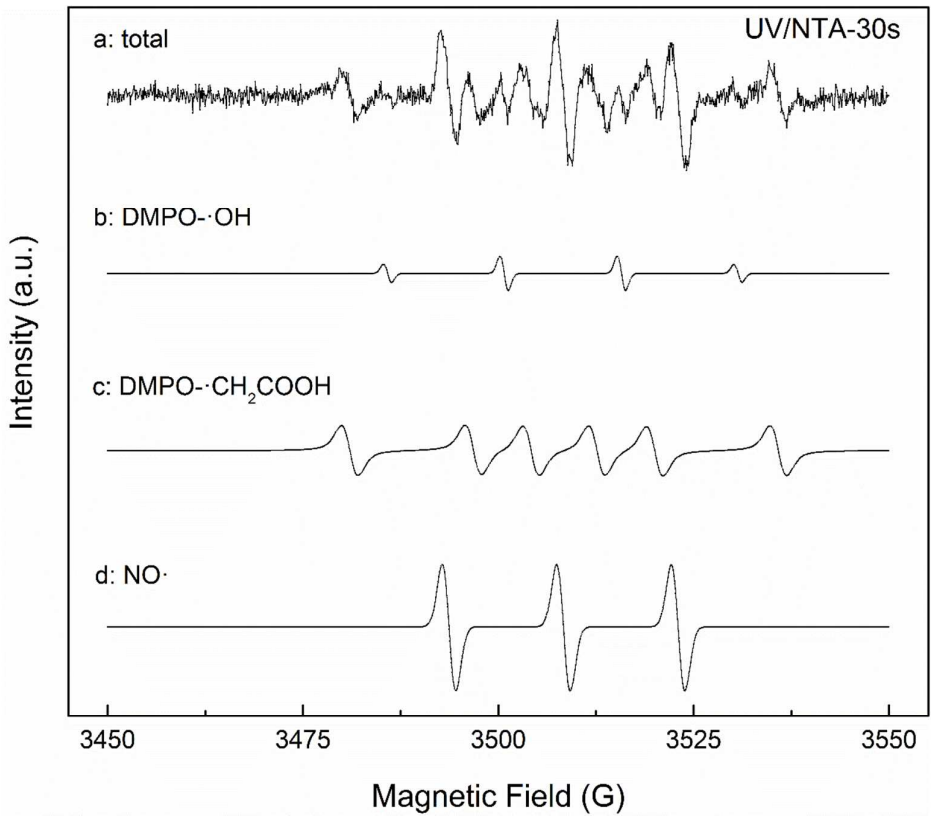

Figure S11. Simulation of various radicals trapped by DMPO in UV/NTA process after 30 s irradiation: (a) total ESR signal; (b) simulation of DMPO-·OH; (c) simulation of DMPO-·CH_2COOH ; (d) simulation of NO·.

3.3. Model compound study

Table S2. Abbreviation and chemical structure of model compounds.

Abbreviation	Name	Chemical structure
NTA	nitrilotriacetic acid	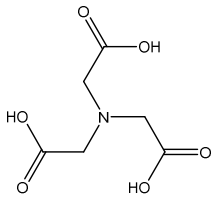
IDA	iminodiacetic acid	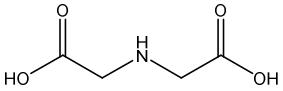
EDTA	ethylenediaminetetraacetic acid	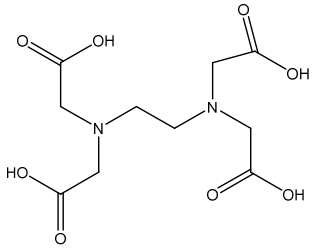
EDDA	ethylenediaminediacetic acid	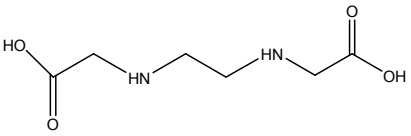
Cit	citric acid	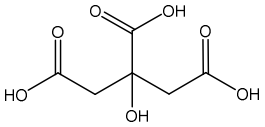
MGDA	methylglycinediacetic acid	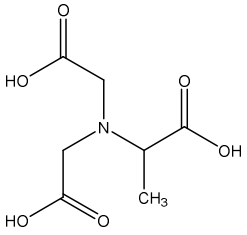
EDDS	ethylenediaminedisuccinic acid	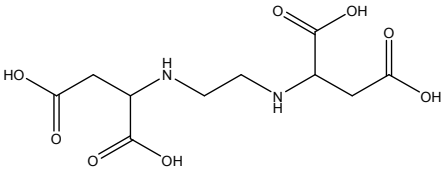
Gly	glycine	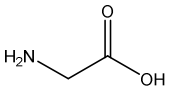

Oxa	Oxamic acid	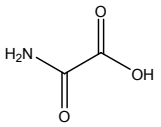
Oxalic acid	Oxalic acid	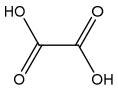

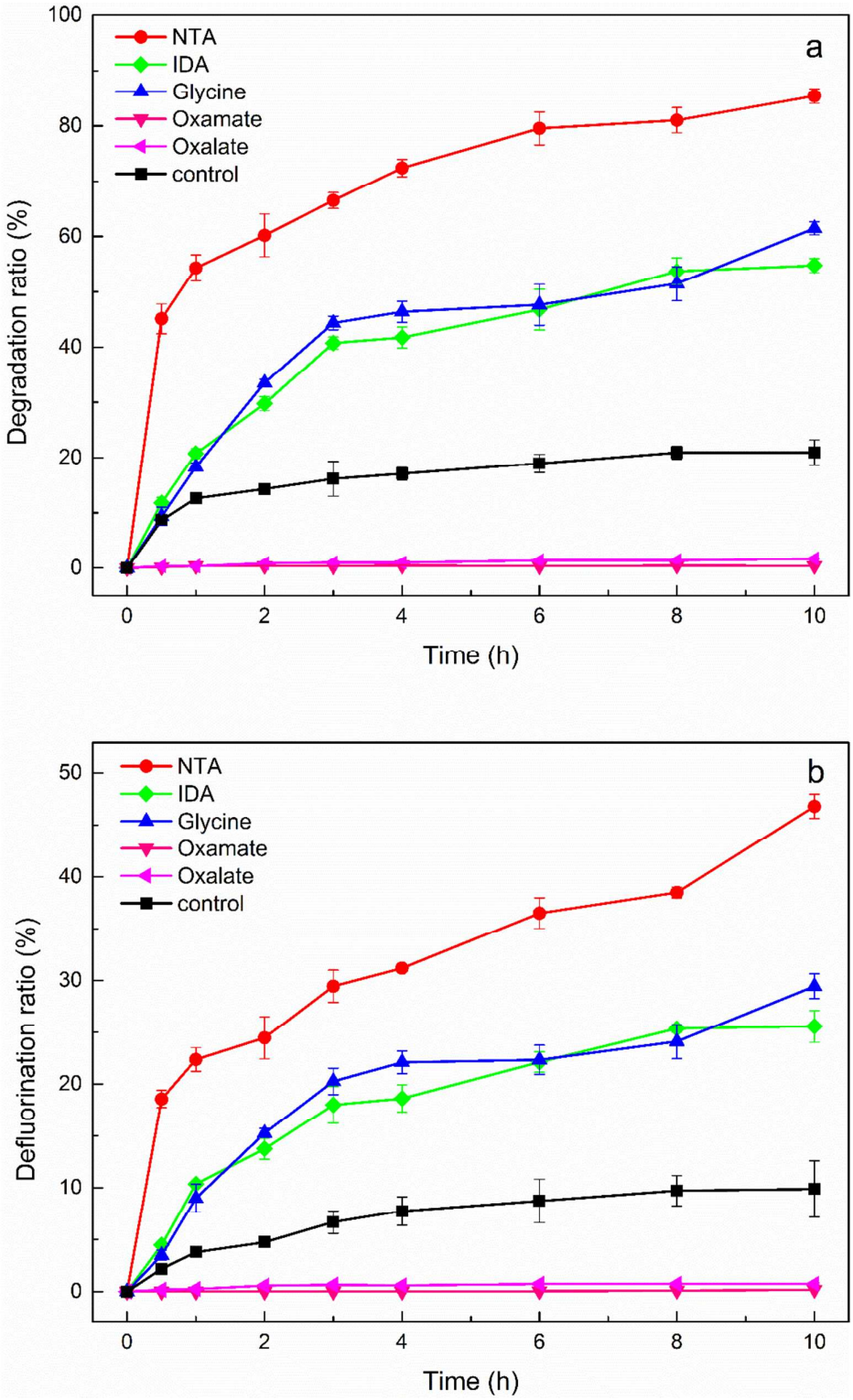

Figure S12. The time profiles of PFOS degradation (**a**) and defluorination (**b**) in the presence of NTA and its degradation products (IDA, glycine, oxamate and oxalate): PFOS (0.01 mM), NTA and the products (2 mM), UV irradiation, N_2 saturated, pH (10.0). Error bars represent standard

deviations of triplicate assays.

3.4. Effect of NTA concentration

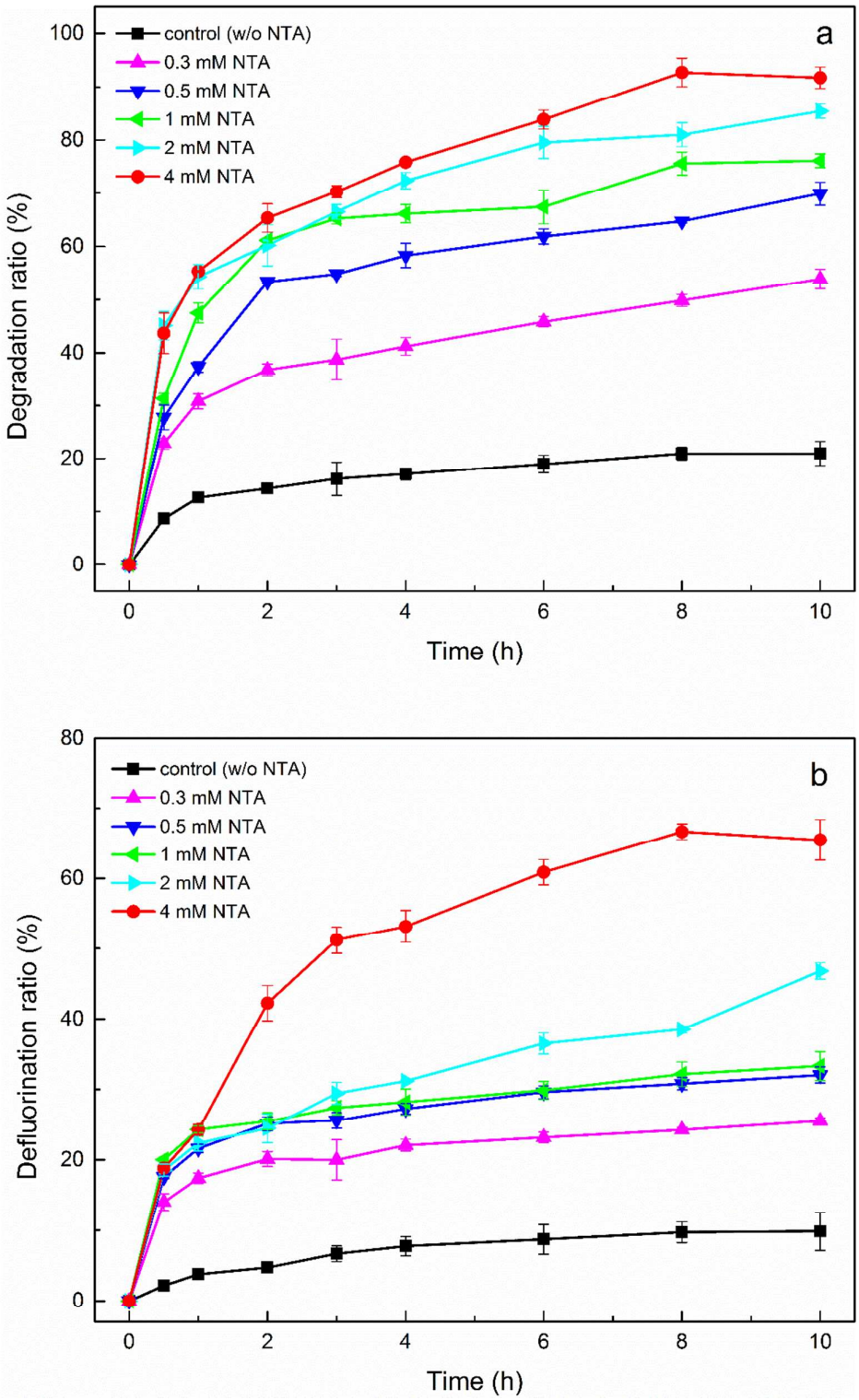

Figure S13. The effect of NTA concentration on the degradation (**a**) and defluorination (**b**) of

PFOS: PFOS (0.01 mM), UV irradiation, N_2 saturated, pH (10.0). Error bars represent standard deviations of triplicate assays.

The effect of NTA concentration on the degradation and defluorination of PFOS is shown in **Fig. S13**. As the concentration of NTA increased from 0 to 4.0 mM, the 10-h degradation ratio of PFOS increased from 20.9% to 91.7% and the 10-h defluorination ratio of PFOS increased from 9.9% to 65.5%. This result was expected since increasing the NTA concentration should lead to more efficient scavenging of ·OH, which, in turn, resulted in a higher steady-state concentration of e_{aq}^- and a more facile degradation of PFOS. By adding 4.0 mM NTA, the degradation ratio of PFOS after 8 h had exceeded 90%. Therefore, UV/NTA process can be a promising strategy for the remediation of PFOS.

References

1. Yamamoto, T.; Noma, Y.; Sakai, S.-I.; Shibata, Y. Photodegradation of perfluorooctane sulfonate by UV irradiation in water and alkaline 2-propanol. *Environ. Sci. Technol.* **2007,** *41* (16), 5660-5665.
2. Park, H.; Vecitis, C. D.; Cheng, J.; Choi, W.; Mader, B. T.; Hoffmann, M. R. Reductive Defluorination of Aqueous Perfluorinated Alkyl Surfactants: Effects of Ionic Headgroup and Chain Length. *J. Phys. Chem. A* **2009,** *113* (4), 690-696.
3. Yang, S. W.; Cheng, J. H.; Sun, J.; Hu, Y. Y.; Liang, X. Y. Defluorination of Aqueous Perfluorooctanesulfonate by Activated Persulfate Oxidation. *PLoS One* **2013,** *8* (10), 10.

4. Jin, L.; Zhang, P. Y.; Shao, T.; Zhao, S. L. Ferric ion mediated photodecomposition of aqueous perfluorooctane sulfonate (PFOS) under UV irradiation and its mechanism. *J. Hazard. Mater.* **2014,** *271*, 9-15.